Direct observation of proton transfer in ice Ih using femtosecond spectroscopy

R. L. A. Timmer,* M. J. Cox, and H. J. Bakker

FOM-institute for Atomic and Molecular Physics,

Science Park 104, 1098 SG Amsterdam, The Netherlands

E-mail: r.timmer@amolf.nl

Abstract

We studied proton transfer in ice samples containing the photo-acid HPTS and the base sodium-formate using femtosecond pump-probe spectroscopy. Pump pulses, centered at a wavelength of 400 nm, electronically excited the photo-acid molecules which released their protons. These protons subsequently traveled from the photo-acid through the ice lattice to the base and were observed as they arrived at the base using the transient absorption of an infrared probe pulse. Both the temperature and concentration dependence of the proton transfer dynamics were modeled using a discrete set of two intrinsic transfer rates, associated with short and long range proton transfer, respectively. Proton transfer in configurations where the acid and base were separated by up to about two water molecules, was found to occur on a $\sim$1 ps timescale for all temperatures (240-270 K). Long range direct proton transfer through water wires of about four water molecule length was found to occur on a $\sim$300 ps timescale for 270 K. This latter process was observed to slow down significantly with decreasing temperature, with an activation energy of $\sim$80 kJ/mol.

Introduction

Hexagonal ice Ih is the most common form of ice on earth. One of the outstanding properties of ice Ih is its relatively high proton mobility. This mobility is important since it forms the basis of most of the anomalous mechanical and electrical properties of ice. That protons can be mobile in ice is in fact quite surprising, because in a perfect ice crystal the hydrogen atoms are expected to be completely immobilized. Therefore the proton mobility is believed to result from the presence and rapid migration of particular defects of the ice lattice.

Whereas liquid water consists of a wide variety of different hydrogen bond distances, strengths and angles, the structure in ice is much more rigid. The molecules in ice Ih form nearly homogeneous hydrogen bond connections with all four of their neighbors at directions close to the tetrahedral angle (109.5°). This tetrahedral arrangement causes the open structure of ice Ih and explains its relatively low density compared to water (0.92 g/cm^3 vs 1.00 g/cm^3).

The tetrahedral arrangement of hydrogen bonds in ice allows for a total of six different orientations of the two hydrogen atoms of the water molecule. Ice Ih has a proton-disordered arrangement as in various other ice polymorphs. In general the orientation of the molecules is determined by the so called Bernal-Fowler ice rules.[1] These rules state that each oxygen atom is connected to two nearby hydrogen atoms and that on each connection between two oxygen atoms, exactly one hydrogen resides. Deviation from these rules can lead to ionic and orientational (Bjerrum[2]) defects. If a proton moves along the hydrogen bond to a neighboring water molecule, the first rule is violated and a pair of OH^- and H_3O^+ ions are created. If a hydrogen atom rotates around the oxygen it is covalently bound to, then the second rule is violated resulting in a pair of Bjerrum L and D defects.[3]

According to Jaccard theory[4] both types of defects contribute to the long range conduction of protons in ice. Intermolecular proton transfer, where a proton hops to the next water molecule is mediated by the migration of ionic defects while intramolecular proton transfer, where a proton moves around the oxygen while staying on the same molecule, is mediated my the migration of Bjerrum defects. In general, such a proton hopping relay cannot continue indefinitely and stops

after a certain distance[5] depending on the local arrangement of the 'water wire'.

The number of defects in ice depends on various factors such as the type of ice, the temperature, and the presence of solutes. For example, going from hexagonal ice Ih to the cubic phase (Ic), the protons become more ordered. At lower temperatures, the number of defects decreases and the ice becomes more structured. The introduction of acidic molecules in the ice creates excess protons in the form of ionic H_3O^+ defects. Similarly, ionic OH^- defects are obtained by adding base molecules. Finally, molecules that do not fit into the periodic ice lattice, act both as sources of lattice defects and as obstacles to defect motion.

Measurements on the conductivity of ice started already in the 19th century when Ayrton and Perry connected two metal electrodes to a block of ice and found an anomalously high conductivity.[6] Later experiments by Eigen[7] seemed to indicate that the proton mobility in ice is much larger than in water. However this increased conductivity was later attributed to surface mobility and not to bulk conduction. Since then a variety of spectroscopic techniques have been used to explore the dynamics of protons and defects in ice crystals. Kunst and Warman[8] used a 50 ns laser pulse to create ionic defects in ice and measured proton mobility using time resolved microwave conductivity measurements. Wooldridge and Devlin[9] used the excitation of the photo-acid 2-naphtol by a mercury lamp to inject protons into deuterated ice and followed the dynamics of protons by monitoring the FTIR spectrum. From their results they estimated the enthalpy of self-ionization in ice to be about 70 kJ/mol.

In recent years the ability to generate and detect ever shorter laser pulses have extended the regime at which we can observe proton transfer down to the sub-ps time range. The excitation of photo-acids with ps laser pulses provide the possibility to release a proton at a very specific instant in time. Huppert[10,11] was among the first to observe excited-state geminate recombination using time-correlated single-photon counting (TCSPC). Using this technique, this group has since performed an excellent and extensive study on a wide variety of proton transfer reactions in both liquid water and ice.[12–16] From their experiments they concluded that proton diffusion in ice is ten times larger than in water of the same temperature.

With TCSPC the time dependent fluorescence signals of a photo-acid are recorded after electronic photo-excitation. The fluorescence spectrum is dependent on the protonation state of the photo-acid and thus reveals whether the proton has been transferred to the solvent or base and/or whether it has recombined. The biggest advantages of TCSPC are its excellent signal to noise ratio and the ability to measure over a long time range (up to 50 ns). However the time resolution of TCSPC is limited to about 35-50 ps.

The use of femtosecond pump-probe spectroscopy increases the time resolution to the sub-ps regime and also allows the possibility to directly probe various other spectral fingerprint bands other than that of the photo-acid. Mohammed and coworkers[17] were the first to use a mid-infrared probe centered at the carbonyl stretching mode to directly monitor the time resolved arrival of the proton at the site of a carboxylic base molecule in liquid water. They also observed intermediate signals that were assigned to various solvated proton complexes. Since then a wide variety of proton transfer reactions in different aqueous solutions and environments have been measured using this technique.[18–21]

In recent work[21] on proton transfer between HPTS and acetate in liquid D_2O, we successfully described the data obtained from a range of temperatures (5-65°C) and base concentrations (0.5-2.0 M) with an extended Smoluchowski[22,23] model which included a distance-dependent reaction rate $k(r)$. From the temperature dependence, it was concluded that this rate $k(r)$ represents *concerted* proton transfer across water wires of different lengths r, connecting acid-base pairs. In such a concerted transfer event, multiple protons move simultaneously, through Grotthus[24,25] hopping, along a pre-formed chain of hydrogen-bonded water molecules. The length and stability of such chains depends strongly on the structure of the water, e.g. the average number of hydrogen bonds.[26]

In this work we extend these measurements to the solid phase and present measurements on the carbonyl stretching mode which directly reflects the excited state proton transfer in ice Ih. Unlike geminate recombination studies, we are sensitive only to those protons that have made a *complete* transfer from acid to base. Because of the high degree of structuring of water molecules in ice and

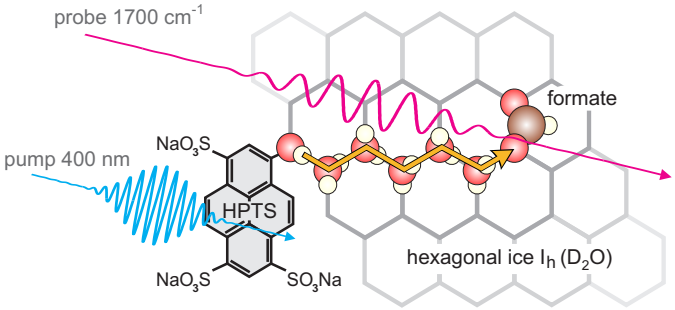

Figure 1: Schematic diagram of the experiment and sample composition. First, the HPTS photo-acid is electronically by the 400 nm pump pulse. Then, the proton transfers through the hexagonal ice by Grotthus[24,25] conduction along a water wire. Finally, the arrival of the proton at the base is detected through the carbonyl stretch, using a 1700 cm^{-1} probe pulse. The size of the HPTS molecule and the hexagonal structure of the ice are approximately to scale (C-C bond length in benzene ring 1.4 Å, O-H$\cdots$O distance in ice 2.7 Å).

because diffusion of acid and base molecules is negligible, it can be expected that proton transfer takes place along pre-formed aqueous water wires. Such water wires are of particular importance in biology where they mediate the transfer of a proton through membrane protein proton channels.[27]

Experimental section

Samples

The samples consisted of D_2O in which was dissolved 20 mM of the photo-acid HPTS (8-hydroxypyrene 1,3,6-trisulfonate, see Figure 1) and 0.10, 0.25, or 0.50 M of the base sodium formate (Na^+HCOO^-). The samples were enclosed in a round cell between two c-cut sapphire windows of 31 mm diameter. The optical path length was set by a 25 μm teflon spacer. The sample cell was placed inside the vacuum housing of a closed-cycle liquid-helium cooled cryostat. The vacuum jacket of the cryostat was equipped with two calcium fluoride windows which allowed optical access to the sample. The cryostat was suspended on a construction above the laser table that allowed the sample cell to be rotated while remaining in the focus of the overlapping pump and probe beams. We will now discuss various considerations in the choice of the samples.

We use D_2O instead of H_2O because the absorption band of the HOH bending mode would otherwise block our spectral observation window around 1700 cm^{-1}. Although the transfer rate of deuterons is expected to be somewhat lower than that of protons, no fundamental difference in the transfer mechanisms is expected.[13]

HPTS is a commonly used photo-acid in the study of reversible excited state proton transfer reactions[10,17,19] with an absorption band around 400 nm. Light at this wavelength can be conveniently generated using the second harmonic of a Ti:sapphire laser. Upon excitation, the HPTS molecule changes its electronic structure[28] leading to a massive increase of its acidity, its pKa reduces from 7.3 to 1.4.[29] This increase in acidity causes the release of a proton to the surrounding water/ice, from where it can travel towards the base molecule. After a few nanoseconds the excited state of the HPTS molecule decays and geminate recombination with the proton occurs. The concentration we use here (20 mM) is high enough to allow for a sufficient pump-probe signal but low enough to prevent the formation of aggregates that would otherwise quench the excited state and hinder the proton release.[28]

As the accepting base, we use sodium formate because it is the smallest of the carboxylic class molecules and will thus cause minimal disruptions to the surrounding ice lattice. The COO group has two stretching modes, symmetric and asymmetric. When the proton arrives at one of the two oxygen atoms, these two modes decouple, shifting the frequency of the carbonyl (C=O) stretch into the region around 1700 cm^{-1}. From the analysis of signals for various base concentrations it was found that the statistical distribution of base molecules in the ice was maintained up to 0.5 M, but not at 1.0 M. Hence it appears that formate does not dissolve uniformly in ice around 1.0 M, but instead is being pushed towards the grain boundaries.

Upon freezing of the sample a dramatic decrease in signal and fluorescence was noticed. This is presumably caused by aggregation of HPTS molecules in the solid phase and was previously observed by the Huppert group.[14] Following their example, we add a small fraction of (deuterated) methanol (0.5%) to the sample which allows the HPTS to better dissolve into the ice lattice and prevents the formation of aggregates. The methanol itself is expected to have negligible effects

on the proton transfer at these low concentrations.[12] From the fact that both the photo-acid and base molecules can be well dissolved into the ice we conclude that their perturbing effects onto the surrounding lattice are limited in range.[30] If this were not the case it would be energetically more favorable for the molecules to be clustered together or pushed into the grain boundaries during the freezing process.

The choice for sapphire windows was made after several calcium fluoride windows broke in the freezing process. Whereas calcium fluoride is very vulnerable to thermal shock, sapphire is much harder and constitutes a very good heat conductor. The only disadvantage is its birefringence which may cause a rotation of the polarization. This drawback is circumvented by using c-cut windows that have the optical axis perpendicular to the cut of the window. The spacing of 25 μm was thin enough to cause minimal scattering of the probe light and the formation of a uniform ice crystal, yet thick enough to allow enough absorption of the pump light.

The cryogenic setup allowed for both heating and freezing of the samples with a temperature stability of about 0.5 K. For the preparation of ice samples we first held the samples at 273 K for about 10 minutes followed by a rapid cooling to a low temperature (240 K) while monitoring the pump-probe signal. The sample was kept at 240 K for about 10 more minutes and then heated up to the desired temperature. Once the sample had reached its desired temperature, a linear spectrum was taken using an infrared spectrometer (Perkin-Elmer). From the linear spectrum we could clearly see that the sample was still frozen from the narrowed peak of the OD stretch vibration of the D_2O solvent. During and after each measurement additional linear spectra were taken to confirm that the sample did not thaw (especially around 270 K).

Pump-probe setup

The experiments were performed using a femtosecond UV-pump, mid-infrared probe laser setup. A commercial Ti:Sapphire system (Quantronix Titan) delivered pulses with a central wavelength of 800 nm at a repetition rate of 1 kHz. This light was split in two parts. One part was frequency doubled in a β-BaB_2O_4 (BBO) crystal to create 100 fs pump pulses at centered at 400 nm. The

remaining part of the 800 nm light was used to generate signal and idler pulses using a white light seeded, BBO based Optical Parametric Amplifier. These pulse were then recombined in a $AgGaS_2$ crystal to yield, through a difference-frequency mixing process, 150 fs probe pulses at a frequency of 1700 cm^{-1}. The pump and probe pulses had pulse energies of 5 μJ and 20 nJ, respectively.

The relative polarizations of pump and probe beams were set to the magic angle (54.7°) to avoid any effects of reorientational diffusion. The probe beam was split in two parts. One part was always preceding the pump and acted as a reference beam to compensate for pulse to pulse fluctuations. The other part was delayed relative to the pump beam using a delay stage (accuracy 30 fs). All beams were overlapped in the sample and both probe beams were detected using a 2×32 pixel MCT (Mercury-Cadmium-Telluride) detector. To avoid the absorption of probe light by gaseous water in the spectral window of the carbonyl vibration, the part of the setup containing the infrared generation and detection was flushed with dry air. The instrument response time was 200 fs.

A 500 Hz chopper wheel was used in the pump beam to measure the pump-induced frequency-resolved transient absorption spectra ($\Delta\alpha$) of samples as a function of time delay between pump and probe. These spectra are calculated by combining the relative transmissions of chopped (T_0) and unchopped (T) probe signals:

$$\Delta\alpha(t,\nu) = T(t,\nu)/T_0(\nu)\,, \tag{1}$$

where t are the delay times between pump and probe, and ν are the probe frequencies.

The pump pulses were focussed in the sample to a relatively large spot size. We took care that the intensity of the pump remained below the threshold where water starts to ionize due to multi-photon absorption, which would create a spectral response from dissolved electrons. To check the absence of this electron response, we also measured a sample where the photo-acid was omitted. The focus of the pump was tuned, using a telescope, well below the point where no more electron signal was detected. The sample was then replaced with one containing the photo-acid.

Cryostat-rotator

Even though the intensity was low enough that no measurable electrons were formed, long term exposure of the sample to UV pump pulses still caused a gradual degradation of the sample quality as witnessed by the decreasing signals and fluorescence. To prevent the signal to be affected by this degradation, the *liquid samples* could be simply rotated in circles inside the pump focus to spread out the damage over a larger area of the sample. This allowed sufficiently long measurement times of about an hour before gradual signal loss could be observed.

The frozen samples were placed inside of large cryostat weighing about 25 kg which was connected to a liquid helium reservoir and a vacuum pump system. Clearly this setup cannot be easily be rotated, especially not while placed on a vibration sensitive laser table. Moreover from earlier test measurements on a smaller, rotating (peltier cooled) ice sample we learned that sample degradation came much sooner for frozen samples than for liquid samples, probably because long timescale diffusion of photo-acids in and out of the pump trajectory could no longer take place. It was observed that a ring of decreased fluorescence was quickly 'burned' along the trajectory of the pump. To make things worse the signal to noise ratio of the rotating ice samples were also much poorer than in the liquid samples even though great care was taken to form homogeneous, clear ice crystals with minimal scattering properties.

To resolve these issues we used a home-built 'cryostat-rotator' (see Figure 2) that was mounted on a frame independent of the laser table. This suspended device is capable of moving around the entire cryostat including the attached hoses while keeping the sample within the focal length of the probe ($\sim$1 mm). To achieve maximum spread of the pump beam across the sample we used a pair of inner and outer gears and rotated the sample along a hypotrochoid trajectory. The x and y positions of this trajectory at time t at an angular speed ω can be described by the following set of parametric equations:

$$x(t) = (R-r)\cos(\omega t) + \delta\cos\left(-\frac{R-r}{r}\omega t\right), \quad (2)$$

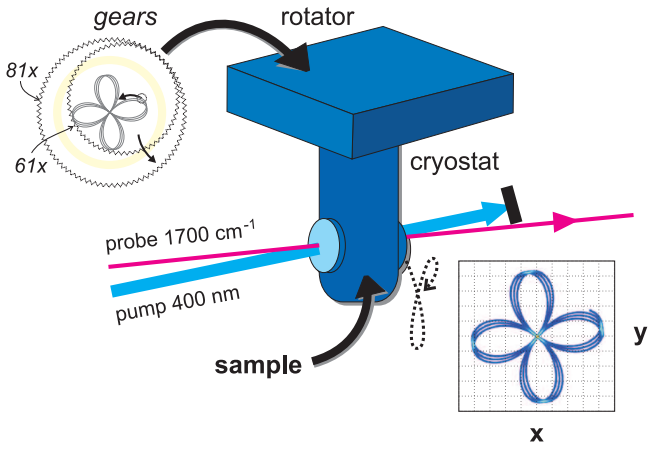

Figure 2: The middle part shows a schematic depiction of the cryostat rotator hanging in the pump-probe setup. The top left shows the outer and inner gears that together create the hypotrochoid trajectory, resulting in a period of almost five thousand rotations. The bottom right picture shows a simulation of the pump intensity distribution across the sample after a few rotations.

$$y(t) \quad = \quad (R-r)\sin(\omega t) + \delta \sin\left(-\frac{R-r}{r}\omega t\right). \tag{3}$$

Here R and r are the radii of the outer and inner gears, respectively, and δ is the offset from the center of the inner wheel to which the rotating cryostat is attached. The number of teeth on the two gears were chosen to be relative prime (61 and 81) in order to achieve the maximum possible period before the trajectory turns back on itself, i.e. after $61 \times 81 = 4941$ rotations. This device allowed us the necessary time of up to six hours per measurement to achieve satisfactory signal to noise ratios.

Results

Decomposition

The pump-probe data sets consist of frequency resolved transient absorptions at various pump probe delay times. A typical data set of ice at 270 K with 0.10 M formate is depicted in Figure 3. Around 1700 cm^{-1} we clearly observe the ingrowing of the carbonyl (C=O) stretch as the proton reaches the formate molecule. Besides this ingrowing feature, the signal also shows a weakly

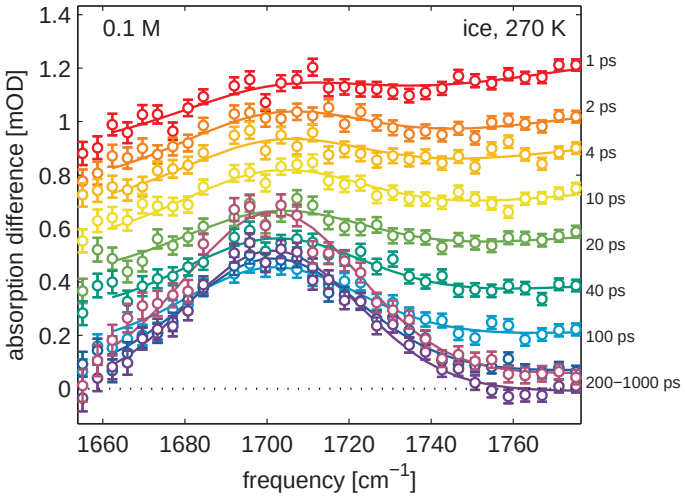

Figure 3: Transient absorption data in the region of the carbonyl stretch mode following excitation of the HPTS photo-acid. The sample contained 0.10 M sodium formate and was held at a temperature of 270 K. The points are the measured absorption difference spectra at various pump-probe delay times (indicated on the right). The data contains contributions of the ingrowing carbonyl stretch mode and a decaying featureless background. The lines show the result of the spectral fitting routine used to extract the population dynamics of the carbonyl stretch.

sloped background band that decreases over time. The origin of this background band is likely the absorption of the (partially) dissolved proton/deuteron.[31]

We extract the dynamics of the ingrowing carbonyl signal i.e. the arrival of the proton at the base, by decomposing the signal into its underlying constituent spectra. From a singular value decomposition[32] on the data matrix $\Delta\alpha(t,\nu)$ we find that it is well described using a two component model. The first two singular values total 88% of the total signal while the subsequent components are $< 1\%$, indicating the noise threshold. We proceed to describe each component as the product of a time evolving population $N(t)$ and a corresponding spectral signature $\sigma(\nu)$:

$$\Delta\alpha(t,\nu) = N_{\mathrm{co}}(t)\cdot\sigma_{\mathrm{co}}(\nu) + N_{\mathrm{bg}}(t)\cdot\sigma_{\mathrm{bg}}(\nu), \tag{4}$$

where the subscripts co and bg signify the carbonyl and (dissolved deuteron) background components, respectively.

To get the spectral signature of the carbonyl stretch, $\sigma_{\mathrm{co}}(\nu)$, we take linear spectra of (frozen)

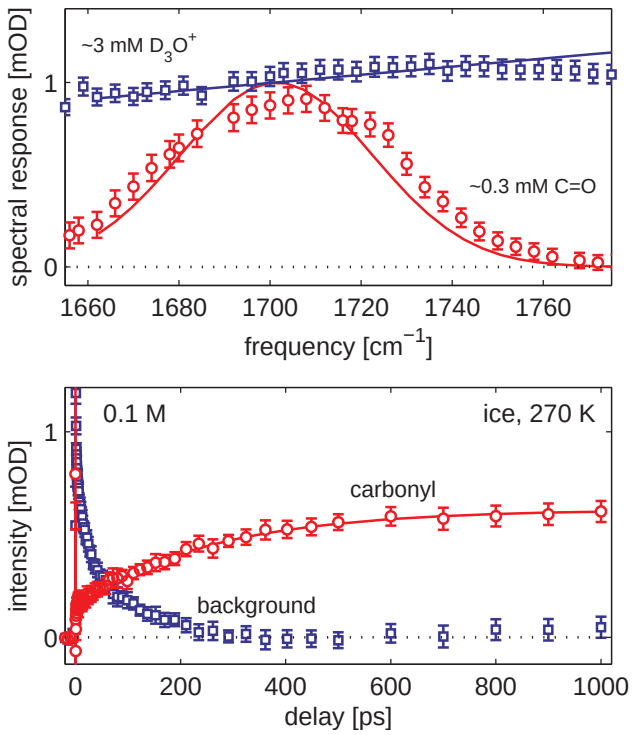

Figure 4: Decomposed spectra (top) and population dynamics (bottom) of 270 K ice with 0.1 M sodium acetate. Top: for comparison the fitted carbonyl spectrum of the pump-probe data (gaussian line) is superimposed with a linear difference spectrum of ∼0.3 mM formic acid and sodium formate (circles). The pump-probe background spectrum (line) is superimposed with a spectrum of ∼3 mM D_3O^+ (squares), obtained by taking a difference spectrum of deuterium iodide (DI) and sodium iodide (NaI). Bottom: The population dynamics of the ingrowing carbonyl peak can be fitted using a bi-exponential of ∼1 and ∼300 ps. The dynamics of the background show a strong peak around zero.

D_2O solutions containing either formic acid or sodium formate. The shape of the difference spectrum is shown in the top of Figure 4. As expected, the difference between the two samples is the presence of a band around 1700 cm^{-1}, belonging to the C=O stretch mode of formic acid. Formic acid is not very strong (pKa 3.7), therefore the difference spectrum does not contain much of the deuteron background band. To determine the response of a deuteron in ice we take a difference spectrum between a strong acid, deuterium iodide (pKa -10) and sodium iodide, resulting in the other spectrum shown in Figure 4.

The linear difference spectra illustrate that indeed the peak is due to C=O and the background is due to deuterons.We approximate the carbonyl stretch with a (unity amplitude) gaussian band

of certain width and central frequency and the background as a single line with unity offset and certain tilt (see top panel of Figure 4). We then fit these two shapes to all delay times where for each iteration we calculate the best fitting linear combination of population amplitudes using:

$$\chi^2(\tilde{N}_{\mathrm{co}},\tilde{N}_{\mathrm{bg}}) = \int d\nu \left(\Delta\alpha(t,\nu) - \tilde{N}_{\mathrm{co}} \cdot \sigma_{\mathrm{co}}(\nu) - \tilde{N}_{\mathrm{bg}} \cdot \sigma_{\mathrm{bg}}(\nu)\right)^2 , \tag{5}$$

The least squares fitting values for $\tilde{N}_{\mathrm{co}}$ and $\tilde{N}_{\mathrm{bg}}$ at each delay time are calculated by equating the derivatives of the above expression with respect to both variables to zero. The fit proceeds to vary the spectra until a global minimum is achieved. The result of this procedure is shown in Figure 3. The fitted spectra σ_{co} and σ_{bg} are shown as lines in the top panel of Figure 4 where it is shown that they are very similar to the linear spectra of the C=O and hydrated deuteron, respectively.

Because the fitted spectra are normalized, the values of $\tilde{N}(t)$ thus obtained are directly proportional to the population dynamics of the carbonyl stretch and background. This also means that we can compare different data sets without the need for any renormalization.

Temperature dependence

The bottom of Figure 4 shows the decomposed population dynamics of both the carbonyl stretch and the background. The carbonyl intensity shows an initial, rapid ($\sim$ 1 ps) ingrowth to about one third of the end level, followed by a slower ($\sim$ 300 ps) ingrowth. These two processes will be designated with the subscripts 0 and 1, respectively.

The rapid ingrowth fraction f_0 has a rate k_0 of about 1 ps^{-1}, which corresponds roughly to the proton hopping time of 1-2 ps that has been measured with NMR techniques.[28,33] We note that f_0 is present both for the ice and supercooled water. This leads us to the assumption that f_0 is caused by directly connected acid-base pairs, since neither in water nor in ice would these configurations experience a diffusion limited reaction rate. This direct connection is formed either between a direct contacting acid-base pair[34] or a (short) wire of intermediate water molecules, aligned such that a concerted (multi proton) jump process can immediately take place between acid and base.

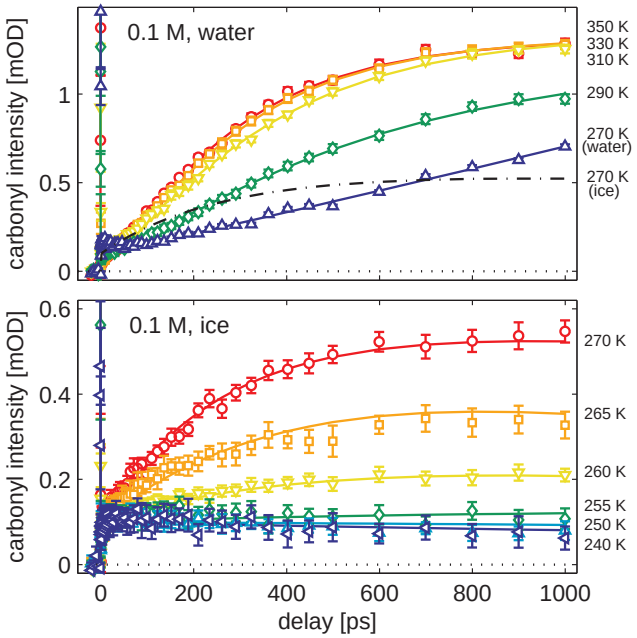

Figure 5: Ingrowth of the carbonyl stretch mode at different temperatures in liquid water (top) and ice (bottom). In the top figure the dashed line shows the ice data for 270 K to compare it more easily to the liquid water of the same temperature. For liquid water at low temperatures there is a delay between the excitation of the photo-acid and the ingrowth of the carbonyl peak. This delay is not present for ice of the same temperature. For higher temperatures the delayed ingrowth disappears and above 330 K no additional changes in proton transfer dynamics is observed. For liquid water the initial, rapid transfer (k_0) is seen to decrease for higher temperatures. For ice, no temperature dependence of this rapid fraction is observed. The long range transfer component (k_1) however is highly temperature dependent and its signal becomes dominated by the back transfer of k_0, below 255 K.

We further note that the fraction f_0 does not increase upon freezing of the sample which would be the case if HPTS and base molecules would start to cluster in the ice formation process. The similarity in amplitude of f_0 in water and ice indicates that the quantum yield of proton release after excitation is also similar in these two systems.

The fitted line in the bottom of Figure 4 shows that the slower proton transfer fraction f_1 with rate k_1 is well described using an ingrowing mono-exponential of about 1/300 ps^{-1}. This finding is in stark contrast to the usual highly non-exponential behavior found for proton transfer in water.[12,17,19] Indeed, if we compare the transfer dynamics between 270 K ice and supercooled water (see top Figure 5), we notice a striking difference. Whereas in water the carbonyl signal

experiences a delayed ingrowth, in ice this signal grows in directly after the excitation. This delayed ingrowth was previously explained[35] as an indirect transfer channel, where the proton is first transferred from the acid to the water solvent and subsequently from the water to the base. It was also noted that this indirect transfer channel is much less noticeable for either higher base concentrations or stronger base molecules. The current observations we show that this type of indirect proton transfer does not occur as readily in ice as it does in water.

Concerning the carbonyl intensity, we note that after the initially slower start, it reaches a much higher end level in water compared to ice. Because we previously argued that the quantum yield of proton release is similar in water and ice (similar fraction f_0), this indicates that the total proton transfer reaction (in particular f_1) reaches a larger number of base molecules in water than in ice (within the HPTS excited state lifetime). This difference may at least in part be caused by the diffusion of the acid and base molecules themselves. In ice the diffusion of acid and base molecules is expected to be practically zero for these timescales. This means that, whereas in water a distant base molecule may still diffuse into the 'reaction radius' of either the acid or dissolved proton, this will not be the case for ice.

For higher temperatures of water, the indirect ingrowth channel diminishes, being almost unnoticeable above room temperature. Above 330 K no further increase in the proton transfer rate is observed. We speculate that, up to this temperature, diffusion of the proton itself is the rate limiting step for the indirect channel of proton transfer in water. This means that in this channel the proton is first released and can then find a base molecule. Conversely, as will be shown below, the indirect channel is completely absent in ice and proton transfer only occurs, provided a direct connection between acid and base is formed. We conclude that for the fraction f_0 this connection exists from the start and the proton can immediately transfer to the base, while for f_1 the formation of this direct connection is the rate limiting step in the whole transfer process. An example of such a (temperature dependent) step would be the reorientation of a 'misaligned' water molecule somewhere along the interconnecting water wire. Once this misaligned molecule has reoriented in a favorable manner, a concerted proton transfer immediately follows that brings the proton from

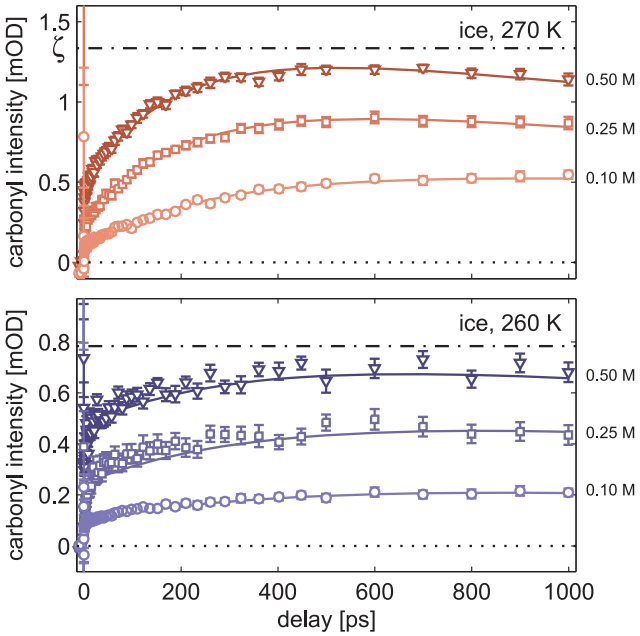

Figure 6: Concentration dependent ingrowth of the carbonyl intensity in ice for 270 K (top) and 260 K (bottom). The circles, squares, and triangles are the data for base concentrations of 0.10, 0.25, and 0.50 M, respectively. Lines are the result of a global fit described in the text. The dash-dotted line indicates the maximum intensity of the carbonyl ingrowth for high concentrations (ζ in Equation 8).

the acid to the base molecule.

For different temperatures of ice (bottom Figure 5, we see that the fraction f_0 stays about the same while f_1 is highly temperature dependent and quickly diminishes with decreasing temperature. Below 255 K the carbonyl intensity mainly shows a decreasing signal. This decrease is in fact present in all data and can be explained by the limited excited state lifetime of the HPTS. When the excited state of the HPTS (or PTS^-) decays, the molecule switches back to being a base and will try to reclaim its proton from the formic acid molecule. This process will occur almost instantaneously for the directly connected base molecules which dominate the signal at lower temperatures. For the higher temperatures the limited excited state lifetime is only observed at later delays when the proton transfer reactions (f_1) are near complete (see bottom Figure 5 265 K).

Concentration scaling

In Figure 6 we see the effects of increasing the concentration of base molecules on the dynamics of the carbonyl ingrowth. First of all we clearly notice that the end levels start to increase for higher concentrations. Furthermore we note that the initial rapid fraction also increases. However these increases are not directly proportional to the increase of base concentration, meaning a doubling of the base concentration does not lead to a doubling of the end level.

In the next section we will introduce a model that is closely related to the Smoluchowski approach,[22,23] of solving the time dependence of the survival probability $S(t)$ of an excited molecule in a random distribution of quenchers. For a time dependent quenching rate $k(t)$ this survival can be written as:

$$S(t) = \exp\left(-\rho\, k(t)\, t\right), \tag{6}$$

where ρ is the concentration of quenchers, in this case the base molecules.

In the absence of excited state decay, the measured carbonyl population $\tilde{N}_{\mathrm{co}}$ and the survival probability are related as:

$$\tilde{N}^{0}_{\mathrm{co}}(t) = \zeta\,(1 - S(t)), \tag{7}$$

where ζ is a scaling constant that normalizes the maximum intensity of the carbonyl stretching mode. This scaling constant is the same for all base concentrations at a certain temperature because it only relates the signal of the carbonyl to the survival probability of the HPTS molecule. In Figure 6 ζ, obtained from the relative scaling of the three concentrations, is indicated as the dash-dotted line above the graphs.

Including the excited state decay k^* of the HPTS molecule can be quite difficult and depends on the exact model for proton transfer. However in the simplest case where the excited state decay is much slower than the proton transfer rate we may decouple the two processes and simply write:

$$\tilde{N}_{\mathrm{co}}(t) = \zeta_{\mathrm{co}}(1 - S(t))e^{-k^* t}. \tag{8}$$

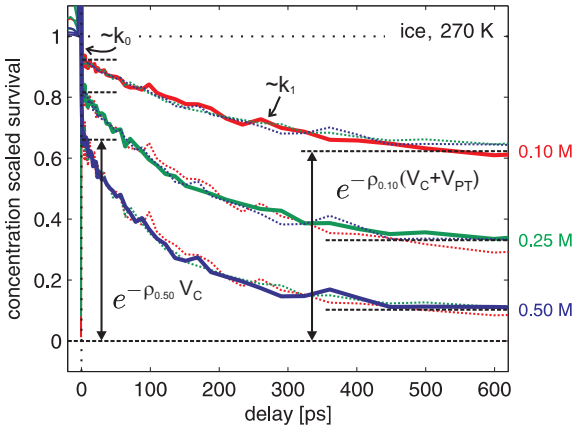

Figure 7: Concentration dependent 'survival probability' in ice at 270 K. Each concentration can be scaled using Equation 9, and overlapped with the other two concentrations, showing that the distribution of base molecules obeys Poisson statistics. At longer delays ($>$ 500 ps) a deviation occurs due to proton transfer back to the photo-acid. The contact and total reaction volumes may be deduced from the graphs using the short ($<$ 10 ps) and long ($>$ 500 ps) time range plateaus indicated with horizontal dashed lines (see Equations 23 and 24).

This equation no longer holds for lower temperatures where the proton transfer rate becomes comparably slow to the excited state decay. In that case we will have to revert to the exact rate equations of all processes involved. For now we will first treat the higher temperatures $>$ 260 K.

Using Equation 6 we can show that the survival probabilities of two concentrations ρ_a and ρ_b should scale as:

$$S_a(t) = \exp\left(-\frac{\rho_a}{\rho_b}\ln(S_b(t))\right), \tag{9}$$

i.e. independent of the time dependent rate $k(t)$.

In Figure 7 we show again the ice data of 270 K for three different concentrations (compare top of Figure 6). However, for this figure all data were divided by $\zeta_{\mathrm{co}} = 1.3$ mOD and flipped vertically according to Equation 7 in order to retrieve the survival probabilities. Superimposed on each survival trace are the two other 'concentration-scaled' survivals (dotted lines). We see that we can quite nicely reproduce all traces: both the end levels but also the rapid ingrowth and the longer time dynamics. This shows that our conceptually simple model is very plausible.

However, as shown in Figure 7, for the lowest concentration at long delay times ($>$ 500 ps) this overlap starts to deviate. In the top panel of Figure 6, for the higher concentrations the back transfer

rate starts to dominate at later delays while for the lower concentrations the carbonyl intensity is still ingrowing. The deviation is caused whenever the decay rate is not proportional to the number of base molecules (as is the case in the presence of back transfer).

Quantitative model

Now that we have established a simple qualitative model for proton transfer in ice, we will expand this model in a more quantitative way. First of all, because we find essentially only two proton transfer rates for the 0.10 M data, it does not make sense to introduce any sort of distance dependent transfer rate as was done for water.[21] Instead we will develop a discrete version of Equation 6 where we will explicitly determine $k(t)$ as being the result of only two (time independent) rates: the rapid transfer rate k_0 and the slower transfer rate k_1. Following the data of Figure 5 and Figure 6 we will allow k_1 to be temperature dependent but not concentration dependent.

The quantitative model thus uses the following assumptions and conventions:

- Each reaction rate k_i corresponds to a certain 'reaction volume' V_i, i. e, the volume containing the reacting base molecules. No explicit distance dependence of this volume with respect to the photo-acid is required. Nevertheless it is obvious that closer volumes will have faster reaction rates and further away volumes will be bigger.

- The average number of base molecules λ_i in a reaction volume V_i is proportional to the overall concentration ρ:

$$\lambda_i \propto \rho \cdot V_i \,. \tag{10}$$

  If the local concentration equals the overall concentration, the reaction volume may be equated to the actual volume and the proportionality turns into an equality. In that case the reaction volume is directly related to the physical size of the volume to which proton transfer takes place. However, if e.g. the local concentration is twice as high as the overall concentration due to clustering of base molecules, the physical volume will be twice as small as determined from the number of reacting base molecules.

- We convert the concentrations to a density ρ using the following:

$$1\text{ M} = 1\text{ mol/dm}^3 = 1\text{ mol} \cdot N_A/(10^{27}\text{Å}^3) = 6.0 \cdot 10^{-4}\text{Å}^{-3}, \tag{11}$$

where $N_A = 6.0 \cdot 10^{23}$ mol^{-1} is Avogadro's number. For ice, where the density of the solvent itself is lower, we scale all base densities and concentrations by the relative densities of ice and water:

$$\rho_{base\ in\ ice} = \frac{\rho_{ice}}{\rho_{water}} \times \rho_{base\ in\ water} \approx 0.92 \times \rho_{base\ in\ water} \tag{12}$$

- The actual number of base molecules n_i in a reactive volume is an integer value and is distributed over all possible configurations according to the Poisson statistics of the expectation value λ_i:

$$P_n(\lambda) = \frac{\lambda^n}{n!} \exp(-\lambda) \tag{13}$$

- The reaction rate to a volume is directly proportional to the number of base molecules residing in that volume. This means the survival probability scales as:

$$S_n(t) = \exp(-nkt) \tag{14}$$

We now introduce the 'Poisson exponential' by combining Equations 13 and 14 and summing over all configurations n:

$$S(t) = \sum_{n=0}^{\infty} \frac{\lambda^n}{n!} \exp(-\lambda) \times \exp(-nkt)\ . \tag{15}$$

Note that this expression also contains $n = 0$ which will be the chance to find no base molecules within the reactive volume. If the concentration is low enough this probability will be high to find these configurations where no reactions take place (rate $0 \times k$). This is essentially what causes the different end levels for lower concentrations: the chance that no proton transfer will occur.

Through some mathematical manipulation and recognizing the Taylor expansion for the exponential function,

$$\sum_{n=0}^{\infty} \frac{f^n}{n!} = \exp(f), \tag{16}$$

we can rewrite Equation 15 as:

$$S(t) = \exp\left[-\lambda(1-e^{-kt})\right]. \tag{17}$$

We now expand the number of reaction volumes and use the fact that the total survival probability is the product of the individual probabilities:

$$S(t) = \prod_i \exp\left[-\lambda_i\left(1-e^{-k_i t}\right)\right] \tag{18}$$

$$= \exp\left[\sum_i -\lambda_i\left(1-e^{-k_i t}\right)\right] \tag{19}$$

This is the most general form of the survival probability of a reactor with i different reaction pathways each containing an average λ_i reactants. As an explicit example we may expand this general form to a distance dependent reaction rate $k(r)$ with a spherically symmetric distribution of reactants. Using $\lambda = \rho \cdot 4\pi r^2 dr$ and going to the continuum limit yields the familiar equation for the Smoluchowski survival in the absence of diffusion:[21]

$$S(t) = \exp\left[-\rho \int dr\, 4\pi r^2 \left(1-e^{-k(r)t}\right)\right]. \tag{20}$$

For the present case we will not assume any distance dependence however, because we previously observed that for the lowest concentration we could only observe two rates. In fact the two rates k_0 and k_1 are so far apart (1 and 1/300 ps^{-1}) that we found it was nearly impossible, let alone meaningful, to fit them with a continuous distance dependence.

That is why we will limit the number of reaction volumes to just two. First, the direct contact volume V_0 and second the 'long distance' proton transfer volume V_1, each with corresponding rates

k_0 and k_1:

$$S(t) = \exp\left[-\rho \cdot \sum_{i=0,1} V_i \left(1 - e^{-k_i t}\right)\right] \tag{21}$$

We note that these equations fulfill the concentration scaling properties of Equation 9, that were used earlier. Furthermore, for long time delays the survival probability goes to

$$S(t \to \infty) = \exp\left[-\rho \cdot (V_0 + V_1)\right] . \tag{22}$$

This equation will go to zero only for high concentrations or large reaction volumes. From the end levels of Figure 7 we can now deduce directly the total reaction volume $(V_0 + V_1)$ of proton transfer at 270 K ice. This reaction volume is most accurately calculated using the end level of the lowest concentration, 0.10 M:

$$V_0 + V_1 = \frac{-\ln(S(t \to \infty))}{\rho} \approx \frac{-\ln(0.63)}{0.10 \times 0.92 \times 6.0 \cdot 10^{-4}\ \text{Å}^{-3}} = 8.4 \cdot 10^3\ \text{Å}^3 \tag{23}$$

The average number of base molecules in this volume at 0.10 M is $\rho \cdot (V_0 + V_1) = 0.46$. From this average we calculate that the (Poisson) chance to find more than one base molecule within the reaction volume is about 8%. This is the reason that a mono-exponential ingrowth fits so well to the data in Figure 4. The higher concentrations of 0.25 and 0.50 M however have on average 1.2 and 2.3 base molecules within the reaction volume. This means that especially the highest concentration shows a distribution of rates (as clarified in Equation 15).

Using the fact that the direct contact rate k_0 is so much faster than k_1 we may assume that the initial rapid ingrowth (up to 4 ps) is predominantly caused by reactions with the direct contact volume. This allows us to estimate separately the direct contact volume. For example, for the concentration of 0.50 M in Figure 7 we measure an initial drop down to about 0.68. This means that the direct contact volume equals:

$$V_0 = \frac{-\ln(0.68)}{0.50 \times 0.92 \times 6 \cdot 10^{-4}\ \text{Å}^{-3}} = 1.4 \cdot 10^3\ \text{Å}^3 . \tag{24}$$

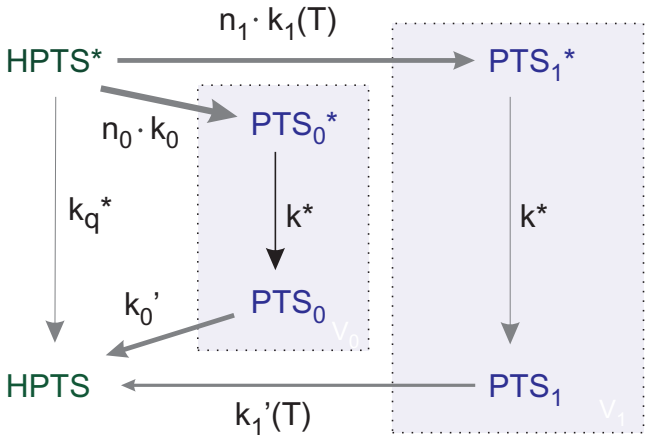

Figure 8: Schematic diagram of the model used for the global fit. Arrows indicate population transfer between different species HPTS*, HPTS, PTS$_i^*$, and PTS$_i$. HPTS and PTS are configurations where the proton reside at the photo-acid or base molecule, respectively. The star (*) indicates that the originating photo-acid is in the excited state. Horizontal/diagonal arrows indicate proton transfer with rates k_0 and k_1, to and from the base molecule. The two boxes indicate the reaction volumes V_0 and V_1, where the base molecules conceptually reside. The reaction rate of proton transfer to a reaction volume is multiplied with the number n_0 or n_1 of base molecules residing in that volume. Vertical downward arrows indicate the excited state decay k^* and k_q^* of the photo-acid, when the proton is at the base or by the photo-acid, respectively.

Of course this means that the other volume $V_1 \approx (8.4 - 1.4) \cdot 10^3$ Å^3 $= 7.0 \cdot 10^3$ Å^3.

Global fit

As noted before, the fact that the proton transfer process at low temperatures becomes comparable to the excited state lifetime, causes deviations from the model of Equation 8. Basically what happens is that when the excited state decays, the proton does not immediately go back to the photo-acid. This process should be included in the complete model. Furthermore we wish to include the possibility that, due to quenching, the excited state lifetime is different depending on the position of the proton, be it at the photo-acid or at the base.[36]

We therefore construct a set of rate equations based on the model described in Figure 8. In this model we keep track of the position of the proton, either at the photo-acid (HPTS) or dissociated from the photo-acid (PTS) and at the carbonyl of the base molecule in any of the two reaction volumes V_0 or V_1. We assign the rates $n_0 \cdot k_0$ and $n_1 \cdot k_1$ to proton transfer from the photo-acid de-

pending on the number of base molecules (n_0 and n_1) residing in the respective reaction volumes. This number is Poisson distributed over different configurations and dependent on the concentration. The super-scripted star in HPTS^* and PTS_i^* indicates the excited state of the photo-acid in this configuration. This excited state is allowed to decay with two different rates k_q^* and k^*, depending on the position of the proton (near the photo-acid or base, respectively). If the proton is near the photo-acid, there is a chance that it will recombine (non-adiabatically) with the HPTS and quench its excited state.[28] If the excited state of the conjugate base decays, it becomes a strong base and it will take up the proton again. This results in the back-going transfer rates k_0' and k_1' that were chosen here to have the same value as the forward going rates. Unlike the forward rates, the backward rates are not multiplied with the number of base molecules n_i in the reaction volume V_i, therefore the total back reaction rate is concentration independent.

The rate equations can be written in the form of a matrix as follows:

$$\frac{d}{dt}\begin{pmatrix} N_{\mathrm{HPTS}^*}(t) \\ N_{\mathrm{PTS}_0^*}(t) \\ N_{\mathrm{PTS}_1^*}(t) \\ N_{\mathrm{PTS}_0}(t) \\ N_{\mathrm{PTS}_1}(t) \\ N_{\mathrm{HPTS}}(t) \end{pmatrix} = \begin{bmatrix} -n_0\cdot k_0 - n_1\cdot k_1 - k_q^* & 0 & 0 & 0 & 0 & 0 \\ +n_0\cdot k_0 & -k^* & 0 & 0 & 0 & 0 \\ +n_1\cdot k_1 & 0 & -k^* & 0 & 0 & 0 \\ 0 & +k^* & 0 & -k_0 & 0 & 0 \\ 0 & 0 & +k^* & 0 & -k_1 & 0 \\ k_q^* & 0 & 0 & +k_0 & +k_1 & 0 \end{bmatrix} \begin{pmatrix} N_{\mathrm{HPTS}^*}(t) \\ N_{\mathrm{PTS}_0^*}(t) \\ N_{\mathrm{PTS}_1^*}(t) \\ N_{\mathrm{PTS}_0}(t) \\ N_{\mathrm{PTS}_1}(t) \\ N_{\mathrm{HPTS}}(t) \end{pmatrix}, \quad (25)$$

with starting conditions $N_i(0) = \delta_{i,\mathrm{HPTS}^*}$, i.e. all protons are initially at the excited photo-acid molecule. The values of n_i are determined by the Poisson distribution and thus concentration dependent.

We solve this set of equations (through matrix diagonalization) as a function of the parameters k_0, $k_1(T)$, k_q^*, and k^* and we keep track of the total (time dependent) sub-populations at the base molecule for any particular configuration of base molecules n_0 and n_1:

$$\tilde{N}_{\mathrm{co}}(n_0,n_1) = N_{\mathrm{PTS}_0^*} + N_{\mathrm{PTS}_1^*} + N_{\mathrm{PTS}_0} + N_{\mathrm{PTS}_1}\,. \quad (26)$$

To get the total population contributing to the carbonyl stretch signal, we weigh each configuration

by the fractional chance that it occurs as given by the Poisson distribution:

$$\tilde{N}_{\mathrm{co}} = \sum_{n_0=0}^{\infty} \sum_{n_1=0}^{\infty} \frac{\lambda_0^{n_0}\, \lambda_1^{n_1}}{n_0!\, n_1!} e^{-\lambda_0-\lambda_1} \times \tilde{N}_{\mathrm{co}}(n_0, n_1)\,, \tag{27}$$

where λ_i is the concentration dependent, average number of base molecules in reaction volume V_i, given by Equation 10.

The time dependent population thus calculated is globally fitted to all concentrations and temperatures where only k_1 is allowed to be temperature dependent. The resulting least-squares fitting parameters are given in Table 1 and Figure 9. Many of the parameter values were already estimated to some degree. We note that the reactive volumes V_0 and V_1 that result from the global fit are close to what had previously been estimated from Figure 7 (Equations 23 and 24), demonstrating that even the simple model of Equation 21 yields reasonable results. What had not yet been estimated was the temperature dependent proton transfer rate through the ice $k_1(T)$. From the Arrhenius plot of Figure 9 we can clearly see a dramatic slowdown with decreasing temperatures. In fact below 255 K the ingrowth of the proton transfer is so slow that the observed dependencies are completely dominated by the excited state decay of the photo-acid.

Table 1: parameter values

$1/k_0$	$(1.1\pm0.5)\cdot10^{0}$ ps
$1/k_1$	$(3\pm0.5)\cdot10^{2}$ ps (@ 270 K)
V_0	$(1.1\pm0.3)\cdot10^{3}$ Å^3
V_1	$(6.4\pm1.2)\cdot10^{3}$ Å^3
$1/k^*$	$(2.6\pm0.5)\cdot10^{3}$ ps
$1/k_q^*$	$(1.2\pm0.5)\cdot10^{3}$ ps

Discussion

The arrival of the proton at the base as measured through the intensity of the carbonyl band has two distinct time scales. The initial rapid ingrowth is presumably caused by direct contact complexes. The associated time of about 1.1 ps is similar to values found by Genosar and coworkers[34] for

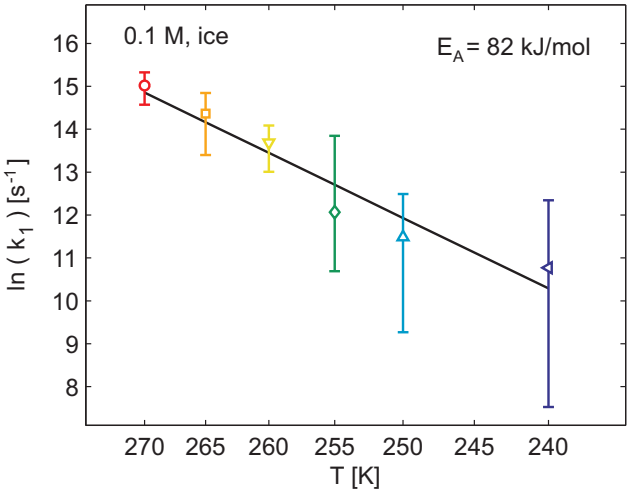

Figure 9: Arrhenius plot of proton transfer rates k_1 in ice with 0.10 M formate, resulting from the global fit. The rate shows a dramatic temperature dependence and was barely distinguishable below 250 K. The rate k_0 showed no significant temperature dependence and is given in Table 1.

direct transfer between HPTS and acetate in water. They described this component with a phenomenological model with a set of two time constants one of which was concentration dependent: 0.7 ps and 1 to 3 ps. From the fitted (direct reaction) volume $V_0 = (1.1 \pm 0.3) \cdot 10^3$ Å^3 we can estimate the total number of water molecules involved. The density of ice I_h is about

$$\frac{0.92\ \mathrm{g/cm^3}}{18\ \mathrm{g/mol}} = 51\ \mathrm{mol/dm^3} = 3.1 \cdot 10^{-2}\ \text{Å}^{-3} = \frac{1 \times \mathrm{H_2O(s)}}{33\ \text{Å}^3}. \tag{28}$$

This means that V_0 contains about 30 water molecules. To get an idea of the distance over which the direct proton transfer reaction takes place, and thus the typical length of the water wires involved, we will make the following simplified assumption about the geometry involved in the experiment. If we assume a spherical distribution of water molecules around a (point source) HPTS molecule we find that the typical direct reaction takes place over a distance of about two water molecules, i.e. $(30/\ {}^4\!/_3\,\pi)^{1/3}$. Of course this distance could be different if we also take into account the volume of the HPTS molecule itself or if we take a different distribution of participating water molecules (e.g. a branching tree of hydrogen bonded water shells[19]). In any case it appears that the direct connection volume is larger than would be expected if this component would only

contain directly contacting acid-base pairs. We speculate that there exist a range of stable structures with the proper arrangement of interconnecting water wires, being able to transfer their proton very quickly to the neighboring base molecule.

We use the same procedure for the reaction volume $V_1 = (6.4 \pm 1.2) \cdot 10^3$ Å^3 and find that it involves about 200 water molecules. Assuming a spherical distribution, we find that the 300 ps proton transfer process k_1 corresponds to a typical water wire length of about 4 water molecules. From the temperature dependence of k_1 we find an activation energy of about 80 kJ/mol for (long range) proton transfer in ice. This number is a bit higher than the numbers found by Leiderman and coworkers,[13] who found a temperature dependent activation energy which was about 65 kJ/mol for 270 K ice and was observed to become smaller with decreasing temperatures. However in that study the geminate recombination without base molecules was probed, so a direct comparison is not possible.

For the short range transfer k_0 we found no appreciable slowdown in the proton transfer speed. This means that the (single) activated process that is essential for the long range transfer k_1 is not present for the short range k_0. We speculate that the long range transfer rate k_1 is rate limited by the favorable reorientation of a single misaligned water molecule in the water wire connecting acid and base. Using NMR techniques, Wittebord and coworkers[37] determined the activation energy for reorientation in ice Ih to be about 55 kJ/mol. This value is somewhat lower than the currently found value of 80 kJ/mol. The high value of this high activation energy suggests that several parallel processes are required to enable the proton transfer, like the reorientation of a water molecule in the ice lattice in combination with a restructuring of the hydrogen-bond network.

Configurations involving the misalignment of multiple water molecules would require a multitude of the activation energy of a single reorientation, which makes them simply too slow to observe here. Therefore we only observe the cases where there are 0 or 1 water molecules misaligned, thus explaining the observation of only two components in the kinetics. The chance to find 'misaligned' water molecules in any particular water wire increases with the length of the chain, which explains why the reaction volume V_0 is smaller than V_1.

For the reaction volume V_1 the average number at the highest concentration (0.5 M) is almost 2 and there is even a $> 12\%$ probability to find 4 or more base molecules in the reactive volume. This means that for this fraction of acid-base pairs the data shows *parallel* reaction pathways to at least 4 base molecules (i.e. four times faster initial rate). By itself the high concentration data could perhaps be explained by using a distance dependent reaction rate. However, this would not agree with the data of 0.10 M where we found essentially only one rate k_1. This single rate is explained by the fact that there is only $< 6\%$ chance to have > 1 base molecule in V_1 at 0.10 M. The observation of a single rate k_1 strengthens the case for a discrete model over that of a continuous (distance dependent) model where there would equally exist a range of rates for all concentrations.

From the concentration scaling procedure we learn that the distribution of base molecules up to 0.5 M behaves according to Poisson statistics. Using Equation 10 we can calculate the average number of base molecules in the reaction volumes for different concentrations. For the highest concentration, measured here, these numbers are $\lambda_0(0.50\text{ M}) = 0.3$ and $\lambda_1(0.50\text{ M}) = 1.9$. For volume V_0 this means that the chance to find more than one base molecule is less than 4%. If we would go to even higher concentrations this percentage would become appreciably high. If no more than one base molecule would physically fit in this contact volume, we will see deviations from the current model. In that case we are no longer in the dilute limit and need to switch to binomial statistics.[19,38]

The model used here, where we show that we can fit our data to a Poisson distributed sum of discrete rates is mathematically not dissimilar from the 'Inhomogeneous Proton-Transfer Kinetics Model' used by the Leiderman and coworkers.[12] They use this model to interpret their TCSPC data on ice samples at short times (i.e. < 1 ns), because they found that the fit quality using the regularly used 'Geminate Recombination Model'[28] was rather poor. The inhomogeneous model essentially assumes a gaussian distribution of rates depending on the distribution of ice around the HPTS molecule.

A big difference with other models on proton transfer in ice (or water), such as the geminate recombination model, is that we do not observe any sign of an indirect proton transfer channel, i.e.

proton release to the ice lattice followed by diffusion of the proton to the base. However we note that the base concentrations used in the TSCPC experiments of Huppert *et al.*[14] are usually in the mM range, which is much lower than we can measure with our infrared pump-probe experiment. For these low concentrations and for their longer time range (up to 50 ns) the diffusion of the proton itself may become an important factor.

All proton transfer reactions in ice were modeled here as a direct transfer from acid to base without intermediate steps. In liquid water this direct transfer pathway also exists, but is accompanied by an indirect transfer mechanism, where the proton may first transfer to the water solvent and subsequently from the water to the base[35] (compare the indirect ingrowth of 270 K water compared to ice in Figure 5). This intermediate step, involving a dissolved proton may be energetically unfavorable in ice,[39] where all molecules are four-fold coordinated and the structure is quite rigid. Conversely, in liquid water the number of hydrogen bonds may vary to accommodate the additional charge of the proton, e.g. by the formation of a stable Eigen[40] (H_3O^+) cation.

After the initial startup time, the total amount of successful proton transfer reactions is higher in water than in ice. Presumably, in ice, proton transfer can only take place for an initially suitable configuration of the water molecules whereas in water these configuration may still adapt, e.g. through the diffusion of acid and base molecules or the reorientation and rearrangement of intermediate water molecules. Also, in liquid water, the proton may first be transferred to solvent and diffuse towards the base.

The difference between proton transfer in water and ice is also noted in theoretical study by Kobayashi and coworkers.[39] They show that whereas the Grotthus[24] type proton transfer mechanism in water is governed in large part by the interconversion of Eigen[40] (H_3O^+) and Zundel[41] ($H_5O_2{}^+$) type water structures, in ice this is no longer the case. Although the density of ice Ih is lower than that of water (0.92 vs 1.0 g/cm^3) the intermolecular O–H$\cdots$O distance is actually a bit smaller (2.75 vs 2.82 Å). Furthermore, in ice all water molecules are four fold coordinated, including the protonated water molecule. The fourth-coordinated water molecule pushes through a repulsive force on the protonated water molecule in ice, thus contributing further to the shortening

of the O–H···O distance to the next water molecule. Due to this shorter distance, the energy barrier for proton transfer is substantially lowered and as a result the distinction between Eigen and Zundel structures does not have much meaning for the transfer dynamics in ice.[39]

Furthermore Kobayashi and coworkers[39] found that the O–H···O distances near the proton are mutually coupled to facilitate the sequential proton transfers in a *concerted fashion*. They found that water molecules up to the fourth solvation shells yield significant contributions to the potential energy surface. They thus conclude that especially the initial part of the proton transfer can be very fast in ice. This conclusion agrees well with our current results that show that direct proton transfer is possible over distances of about four water molecules (either immediately or after the reorientation of a misaligned water molecule). In the current experiment the presence of the base molecule is expected to further influence the potential energy of the proton along the trajectory between acid and base such as to enhance the long range transfer rate in comparison to bulk ice.

In our model we allowed two different excited state decay rates for the bound and unbound states of the HPTS and its proton. The bound rate k_q^* is faster than the unbound rate $1/k^*$, because the proximity of the proton allows it to quench the excited state of the HPTS.[28] Such a difference in excited state lifetime was previously observed by Gopich using time-resolved fluorescence decay measurements of 5-cyano-2-naphthol in DMSO.[36] For our data, the two lifetimes control different aspects of the ingrowth of the carbonyl peak. Whereas the rate k^* may be directly observed as the rate of decay for the low temperature data (see Figure 5), the bound rate k_q^* is only observed indirectly as the decreasing rate of ingrowth due to the depleting source of protons.

Conclusion

We directly observed the arrival of transferred protons in ice from a photo-acid to a base in the time range between 0.2 and 1000 ps. The signature of the transfer is the ingrowth of the carbonyl stretching mode of the base molecule. The dynamics of this mode shows two very distinct time scales of around 1 and 300 ps. Because we can fit the low concentration proton transfer data

with these two timescales alone, we adopt a model with discrete transfer rates. The model can fit higher concentrations of base molecules assuming that the rate is proportional to the number of parallel transfer channels. This number depends on the statistical chance to find one or more base molecules in the reaction volume. Unlike in water we can neglect the diffusion of the protons in ice, because the existence of a 'free' proton complex in ice is energetically unfavorable.

The two transfer rates each correspond to a specific reaction volume. The size of these volumes follows directly from the relative contributions to the total proton transfer process at different concentrations. The fast rate $k_0 = 1$ ps^{-1} corresponds to a volume of about 30 water molecules. Assuming a spherical distribution, this number indicates that it involves base molecules that are connected to the photo-acid with up to two water intermediate water molecules. The second transfer rate $k_1 = 1/300$ ps^{-1} corresponds to a reaction volume of about 200 water molecules which is indicative of proton transfer across water wire lengths of about 4 molecules. This latter rate shows a strong temperature dependence with an activation energy of about 80 kJ/mol. We speculate that this activation energy corresponds to the reorientation of a single misaligned water molecule in the water wire connection between acid and base in combination with a rearrangement of the surrounding hydrogen bond network.

We find a couple of striking differences between proton transfer in ice compared to water. First of all, we find that proton transfer in ice can be described with a discrete set of transfer rates as opposed to a distribution of distance dependent rates like in water. This discrete nature was explained from the more rigid structure of ice, that does not readily allow for the rearrangement and reorientation of 'water wires' or the diffusion of solutes. We observe two classes of transfer rates characterized by the number of defects (0 or 1) of the water wire that connects the acid and the base. Secondly, the proton transfer process in ice was observed to consist of a single concerted process along a water wire between acid in base. This contrasts with proton transfer in supercooled water, where an intermediate step could be observed involving the solvation of the proton as a localized H_3O^+ cation. This difference was explained from the strict four-fold coordination in ice compared the more adaptable hydrogen bond structure in water. Finally, we find concerted proton

jumps in ice over as many as 4 connecting water molecules, much higher than in water (up to 2). This was explained by the higher structure and the increased sphere of influence that the excess proton charge exhibits in ice compared to water.

Acknowledgement

This work is part of the research program of the Foundation for Fundamental Research on Matter (FOM) which is financially supported by the Dutch organization for Scientific Research (NWO). The authors gratefully thank Hinco Schoenmaker and Iliya Cerjak for technical support and Mischa Bonn for helpful comments.

References

(1) Bernal, J. D.; Fowler, R. H. *J. Chem. Phys* **1933**, *1*, 515–548.

(2) Bjerrum, N. *Kong. Danske Vid. Selsk. mat.-fys. Medd.* **1951**, *27*, 56.

(3) Podeszwa, R.; Buch, V. *Phys. Rev. Lett.* **1999**, *83*, 4570–4573.

(4) Jaccard, C. *Helv. Phys. Acta* **1959**, *32*, 89.

(5) Lee, C.-W.; Lee, P.-R.; Kim, Y.-K.; Kang, H. *J. Chem. Phys* **2007**, *127*, 084701.

(6) Ayrton, W. E.; Perry, J. *Proc. Phys. Soc. London* **1877**, *2*, 171–182.

(7) Eigen, M. *Angew. Chem. Intl. Ed.* **1964**, *3*, 1–19.

(8) Kunst, M.; Warman, J. M. *J. Phys. Chem.* **1983**, *87*, 4093–4095.

(9) Wooldridge, P. J.; Devlin, J. P. *J. Chem. Phys* **1988**, *88*, 3086–3091.

(10) Pines, E.; Huppert, D. *Chem. Phys. Lett* **1986**, *126*, 88 – 91.

(11) Pines, E.; Huppert, D.; Agmon, N. *J. Chem. Phys* **1988**, *88*, 5620–5630.

(12) Leiderman, P.; Gepshtein, R.; Uritski, A.; Genosar, L.; Huppert, D. *J. Phys. Chem. A* **2006**, *110*, 9039–9050.

(13) Leiderman, P.; Uritski, A.; Huppert, D. *J. Phys. Chem. A* **2007**, *111*, 4998–5007.

(14) Uritski, A.; Leiderman, P.; Huppert, D. *J. Phys. Chem. C* **2007**, *111*, 8856–8865.

(15) Uritski, A.; Presiado, I.; Huppert, D. *J. Phys. Chem. C* **2008**, *112*, 11991–12002.

(16) Uritski, A.; Presiado, I.; Erez, Y.; Gepshtein, R.; Huppert, D. *J. Phys. Chem. C* **2009**, *113*, 10285–10296.

(17) Mohammed, O. F.; Pines, D.; Dreyer, J.; Pines, E.; Nibbering, E. T. J. *Science* **2005**, *310*, 83–86.

(18) Mohammed, O. F.; Pines, D.; Pines, E.; Nibbering, E. T. *Chem. Phys.* **2007**, *341*, 240–257.

(19) Siwick, B. J.; Bakker, H. J. *J. Am. Chem. Soc.* **2007**, *129*, 13412–13420.

(20) Cox, M. J.; Siwick, B. J.; Bakker, H. J. *Chem. Phys. Chem.* **2009**, *10*, 236.

(21) Cox, M. J.; Timmer, R. L. A.; Bakker, H. J.; Park, S.; Agmon, N. *J. Phys. Chem. A* **2009**, *113*, 6599Ű–6606.

(22) Rice, S. A. *Diffusion Limited Reactions*; Elsevier: Amsterdam, 1985; Vol. 25.

(23) Szabo, A.; Zwanzig, R.; Agmon, N. *Phys. Rev. Lett.* **1988**, *61*, 2496–2499.

(24) de Grotthus, C. J. T. *Ann. Chim.* **1806**, *58*, 54–74.

(25) Agmon, N. *Chem. Phys. Lett* **1995**, *244*, 456.

(26) Brewer, M. L.; Schmitt, U. W.; Voth, G. A. *Biophys. J.* **2001**, *80*, 1691Ű1702.

(27) Luecke, H.; Richter, H.-T.; Lanyi, J. K. *Science* **1998**, *280*, 1934–1937.

(28) Agmon, N. *J. Phys. Chem. A* **2005**, *109*, 13–35.

(29) Lakowicz, J. R. *Principles of Fluorescence Spectroscopy*; Springer, 1999.

(30) Koga, K.; Tanaka, H. *J. Chem. Phys* **1996**, *104*, 263–272.

(31) Kim, J.; Schmitt, U. W.; Gruetzmacher, J. A.; Voth, G. A.; Scherer, N. E. *J. Chem. Phys* **2002**, *116*, 737–746.

(32) Nash, J. C. *Compact Numerical Methods for Computers: Linear Algebra and Function Minimisation, 2nd ed.*; Bristol, England, 1990; pp 30–48.

(33) Luz, Z.; Meiboom, S. *J. Am. Chem. Soc.* **1964**, *86*, 4768–4769.

(34) Genosar, L.; Cohen, B.; Huppert, D. *J. Phys. Chem. A* **2000**, *104*, 6689–6698.

(35) Cox, M. J.; Bakker, H. J. *J. Chem. Phys* **2008**, *128*, 174501.

(36) Gopich, I. V.; Solntsev, K. M.; Agmon, N. *J. Chem. Phys* **1999**, *110*, 2164–2174.

(37) Wittebort, R. J.; Usha, M. G.; Ruben, D. J.; Wemmer, D. E.; Pines, A. *J. Am. Chem. Soc.* **1988**, *110*, 5668–5671.

(38) Siwick, B. J.; Cox, M. J.; Bakker, H. J. *J. Phys. Chem. B* **2008**, *112*, 378–389.

(39) Kobayashi, C.; Saito, S.; Ohmine, I. *J. Chem. Phys* **2000**, *113*, 9090–9100.

(40) Eigen, M.; Maeyer, L. D. *Proc. Royal. Soc. London A- Math. Phys. Sci.* **1958**, *247*, 505–533.

(41) Hadzi, D.; Bratos, S. *The Hydrogen Bond*; Elsevier, 1976; Vol. 2.

Table of Contents graphic

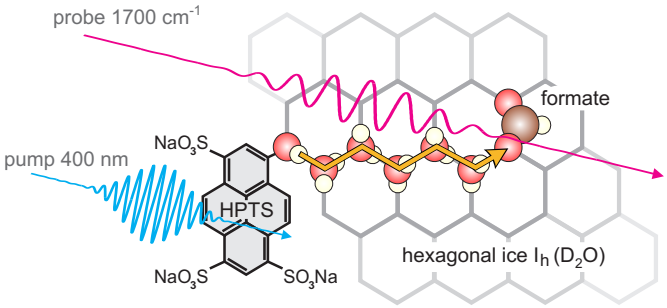

Figure 10: Schematic representation of the pump-probe experiment used to study proton transfer in ice between a photo-acid (HPTS) and a base (formate).